

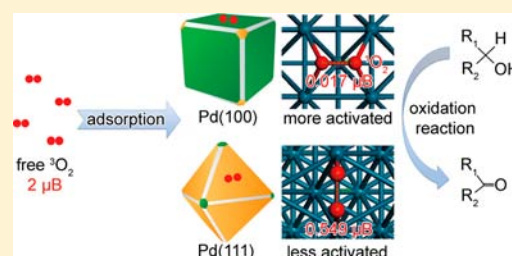
Surface Facet of Palladium Nanocrystals: A Key Parameter to the Activation of Molecular Oxygen for Organic Catalysis and Cancer Treatment

Ran Long,^{†,‡} Keke Mao,[‡] Xiaodong Ye,[‡] Wensheng Yan,[§] Yaobing Huang,[‡] Jianyong Wang,[‡] Yao Fu,[‡] Xisheng Wang,[‡] Xiaojun Wu,^{†,‡,||} Yi Xie,^{†,‡} and Yujie Xiong^{*,†,‡}

[†]Hefei National Laboratory for Physical Sciences at the Microscale, [‡]School of Chemistry and Materials Science, [§]National Synchrotron Radiation Laboratory, and ^{||}CAS Key Laboratory of Materials for Energy Conversion, University of Science and Technology of China, Hefei, Anhui 230026, P. R. China

Supporting Information

ABSTRACT: In many organic reactions, the O₂ activation process involves a key step where inert ground triplet O₂ is excited to produce highly reactive singlet O₂. It remains elusive what factor induces the change in the electron spin state of O₂ molecules, although it has been discovered that the presence of noble metal nanoparticles can promote the generation of singlet O₂. In this work, we first demonstrate that surface facet is a key parameter to modulate the O₂ activation process on metal nanocrystals, by employing single-facet Pd nanocrystals as a model system. The experimental measurements clearly show that singlet O₂ is preferentially formed on {100} facets. The simulations further elucidate that the chemisorption of O₂ to the {100} facets can induce a spin-flip process in the O₂ molecules, which is achieved via electron transfer from Pd surface to O₂. With the capability of tuning O₂ activation, we have been able to further implement the {100}-faceted nanocubes in glucose oxidation. It is anticipated that this study will open a door to designing noble metal nanocatalysts for O₂ activation and organic oxidation. Another perspective of this work would be the controllability in tailoring the cancer treatment materials for high ¹O₂ production efficiency, based on the facet control of metal nanocrystals. In the cases of both organic oxidation and cancer treatment, it has been exclusively proven that the efficiency of producing singlet O₂ holds the key to the performance of Pd nanocrystals in the applications.



INTRODUCTION

The manipulation over the electron states of molecules holds the key to modulating molecular behavior in various chemical and biological systems. For instance, activation of molecular oxygen (O₂) on the surface of heterogeneous catalysts plays a central role in a wide variety of oxidation reactions, such as epoxidation¹ and CO,^{2,3} hydrocarbon,^{4,5} alcohol,^{6–8} and glucose oxidations.^{9–11} In the organic systems, the interaction of organic molecules with O₂ is essentially limited by the spin state of O₂, caused by spin-conservation restrictions. It is well-known that the ground state of O₂ is in a triplet form (³Σ), and as a result, the chemical reactions which occur between singlet organic molecules and triplet O₂ to produce new singlet compounds are forbidden by the Wigners spin selection rule.^{12,13} Thus the triplet multiplicity of O₂ makes most oxidation reactions of organic molecules kinetically inhibited at relatively low temperatures. In principle, a key step is the excitation of inert ground triplet O₂ to highly reactive singlet O₂ (¹O₂: ¹Δ and ¹Σ), during the process of O₂ activation in many organic reactions. However, the direct excitation of triplet to singlet O₂ is not feasible, according to the spin selection rule.

For the reason above, it is necessary to select appropriate media to overcome this spin limitation. In the past decades, it

has been a common route to generate singlet O₂ by the photosensitization in which the excited triplet structures of dye molecules or semiconductor nanocrystals transfer energy from excitons to O₂ and thus change its electron spin state (i.e., a spin-flip process).^{13–15} The efficiency of this method is highly dependent on the singlet–triplet splitting energy and exciton lifetime. In recent years, there has been significant progress to discover that singlet O₂ can be produced in the presence of noble metal nanoparticles.¹⁶ As localized surface plasmon resonance (LSPR) is an optical phenomenon commonly observed in many noble metal nanoparticles, LSPR has been considered as a major source to harvest solar energy into reaction systems.¹⁶ Although the success in the metal system was tentatively explained by this “LSPR sensitization” mechanism, it is still not well understood why the spin-flip process could occur during the LSPR energy harvesting. The fundamental question is: What factor induces the change in the electron spin state of O₂ molecules with the assistance of metal nanoparticles? Thus it is imperative to explore the detailed mechanism behind what will in turn enable greater under-

Received: December 6, 2012

Published: February 7, 2013

standing on the generation process of singlet O_2 with metal nanoparticles and lead to the capability of designing optimal nanocatalysts for related organic reactions. In this article, we first employ single-facet palladium (Pd) nanocrystals as a model system to investigate the detailed mechanisms. We intend to select Pd nanocrystals with the size range of 6–21 nm as the research focus, as it has been demonstrated that the LSPR of small Pd nanoparticles is located in the UV spectral range.¹⁷ In the consideration that UV light has very minimal thermal effect, we can specifically perform characterizations under UV illumination source to reveal whether LSPR is the major contributor to the spin–flip process, while excluding the possibility that light illumination may cause an increase in solution temperature (i.e., thermal effect).

In addition to the possible role of the LSPR in oxygen activation that the literature proposed, the adsorption of small molecules to crystallographic facets may also be a critical factor to the O_2 activation, as the adsorption process represents the most important step for the interactions of metal surface with molecules. As demonstrated in the $O_2Au_n^-$ system, electron transfer from metallic clusters to O_2 may occur upon the binding of O_2 to metal atoms, which eventually causes the activation of O_2 via molecular adsorption.¹⁸ When the investigation is focused on the system of nanoscale crystals (which is actually a more interesting system than the clusters, owing to its wide applications), various surface facets on the crystals may have a huge impact on the molecular adsorption process due to their different atomic arrangements. Thus the single-facet nanocrystals would be an ideal model system for investigating the metal–molecule interactions. In our investigation, two types of nanocrystals with different surface facets are used: cubes enclosed by $\{100\}$ facets and octahedrons by $\{111\}$ facets. The comparison on the yields of singlet O_2 , characterized by probe molecules in the presence of various scavengers, exclusively demonstrates that singlet O_2 is preferentially formed on $\{100\}$ facets. Both the simulations and characterizations further elucidate that O_2 is more activated on the $\{100\}$ facets via chemisorption, indicated by bond length increase and magnetic moment decrease. The spin–flip process occurs via electron transfer from metal surface to O_2 during the preferential chemisorption of O_2 to the $\{100\}$ facets. As facet control enables to tuning the capability of activating O_2 , we have been able to demonstrate that the surface facet of metal nanocrystals is a critical parameter to designing catalysts for organic oxidation and therapy agents for cancer treatment.

■ EXPERIMENTAL SECTION

Nanocrystal Synthesis. The Pd nanocubes were synthesized according to our previously reported protocol.¹⁹ The size of nanocubes can be controlled via oxidative etching or reaction time. The Pd octahedrons were synthesized by tuning reaction kinetics. The detailed protocols are shown in Supporting Information (SI).

TMB Measurements. 20 μ L of 3,5,3',5'-tetramethyl-benzidine (TMB) aqueous solution (50 mM) was mixed with 2 mL of HAC/NaAc buffer solution (0.2 M:0.2 M), and 50 μ L of aqueous suspension of different palladium nanocrystals (0.99 mg/mL for nanocubes and 0.35 mg/mL for octahedrons) was then added into the mixture solution at 10 °C. The concentrations of nanocrystals were selected to maintain the surface atoms of samples equivalent. The samples were taken at different times for UV–vis measurements. UV–vis absorption spectra were collected using an Agilent Varian Cary 60 spectrophotometer. The measurements were performed in various gas environments. In order to verify the type of active oxygen species, different scavenger molecules were added into the solution prior to the UV–vis

measurements: (1) carotene (0.5 mg, excess due to the water insoluble and easily oxidized nature of carotene); (2) mannite (50 mM, 100 μ L); (3) catalase (4000 unit/mL, 100 μ L); (4) superoxide dismutase (SOD, 4000 unit/mL, 100 μ L), respectively.

4-oxo-TMP Measurements. 50 μ L of aqueous suspension of different palladium nanocrystals (0.85 mg/mL for nanocubes and 0.3 mg/mL for octahedrons) was mixed with 500 μ L of 2,2,6,6-tetramethyl-4-piperidone hydrochloride (4-oxo-TMP, TCI, T1147–25g) solution (50 mM). The concentrations of nanocrystals were selected to maintain the surface atoms of samples equivalent. The solution was then characterized with a JES-FA200 electron spin resonance (ESR) spectroscopy at 20 °C. The measurements were performed in different chemical environments and incident light conditions. The Xe lamp irradiation was carried out by USHIO Optical Modulex SX-U1501XQ (500 W).

Glucose Oxidation. The oxidation reactions were carried out in a three-neck flask (50 mL) and heated in an oil bath (equipped with a reflux condenser and a magnetic Teflon-coated stirring bar). Typically, glucose (15 mM) in aqueous solution was heated to the required temperature with O_2 (10 mL/min) for 10 min. Subsequently, the desired amount of catalyst was injected into the solution. The mixture was maintained at pH \approx 9 by adding NaOH solution (1 M), and the reactions were typically carried out for 2 h. After a certain period of the reaction, the mixture was centrifuged, and the liquid solution was completely decanted. For the identification and analysis of the products, LC-20AD high-performance liquid chromatography (HPLC) was employed. HPLC was performed on a column of inertsil ODS-3 (GL science Inc., Kyoto) using an methanol in 0.005 M aqueous solution of sulfuric acid (5:95, v/v), at a flow rate of 1.0 mL/min at 30 °C. In order to investigate the effects of light, different incident light conditions were introduced to the experiment. The Xe lamp irradiation was carried out by SolarEdge700 (300 W) with a visible transmitting filter ($\nu > 400$ nm) and a UV reflecting filter ($\nu < 380$ nm).

Cancer Treatments. Human epithelial cervical cancer Hela was maintained in DMEM medium supplemented with 10% fetal bovine serum at 37 °C under 5% CO_2 in a humidified incubator. Hela cells were harvested using commercial trypsin enzyme. The viable cell concentrations were determined by Trypan blue staining (0.4%). In each well of a 96-well plate, 10 000 viable cells were plated. After 24 h in 5% CO_2 at 37 °C, the medium was replaced with 100 μ L of the same serum-free DMEM without phenol red with nanoparticles at the same concentration in terms of surface atoms (425 μ g/mL for nanocubes and 150 μ g/mL for octahedrons, respectively). A positive control containing the same number of cells in the same medium without any nanoparticles was used. The plates were incubated for 24 h for Hela cells. At the end of the incubation, the cells were washed with serum-free DMEM without phenol red. Then 100 μ L of serum-free DMEM without phenol red and 20 μ L of MTT in PBS solution (5 mg/mL) were added to each well, and the plates were incubated at 37 °C for another 2 h. After incubation, supernatants were removed, and 150 μ L of DMSO was added. The samples were shaken gently until the purple formazan crystals were thoroughly dissolved. The absorbance was measured using a microplate reader (iMark, Bio-Rad) at 595/655 nm, and the percent viability was calculated from the following equation $A_{\text{sample}}/A_{\text{control}} \times 100$.

NEXAFS Measurements. The O K-edge X-ray absorption fine structure spectroscopy (XAFS) was measured at the U7C station of National Synchrotron Radiation Laboratory (NSRL) China. The storage ring of the NSRL was operated at 0.8 GeV with a maximum current of 200 mA. The substrates were silicon chips which were deposited by gold in order to overlay the oxide layer and then ultrasonic cleaned by water.

Computational Methods. Spin-polarized density functional theory (DFT) calculations were performed using the Vienna ab initio simulation (VASP) package to explore the adsorption of molecular O_2 on Pd nanocrystal surface. The frozen-core all-electron projector augmented wave (PAW) method was used to describe electron–ion interaction during the calculation, with the generalized gradient approximation with the Perdew–Burke–Ernzerhof (PBE) functional

for exchange–correlation energy. The dipole correction was considered. An energy cutoff of 500 eV was used for the plane-wave expansion of the electronic wave function. The Pd surface was modeled with 4×4 slab with five layers, and the vacuum region was set to 15 Å. Two bottom layers of the five layers were fixed to the bulk positions during the relaxation. In the relaxation, the force convergence criterion was set to 0.01 eV/Å, and the energy convergence criterion was 10^{-4} eV. The first Brillouin zone was sampled with $3 \times 3 \times 1$ k -points using γ center scheme.

RESULTS AND DISCUSSION

In our investigations, the capabilities of Pd nanocrystals in activating O_2 are initially demonstrated with the measurements using probe molecules. We have employed the TMB reaction as a model system to examine the interaction of O_2 with Pd nanocrystals in various environments. The agent of TMB has been widely used as a chromogenic substrate in staining procedures in immunohistochemistry as well as a visualizing reagent used in enzyme-linked immunosorbent assays, as TMB molecules can be oxidized by relatively strong oxidants to yield colored products. As the reaction scheme (Figure S1) illustrates, the TMB can be oxidized into two products with absorption wavelengths at 370 and 652 nm (one-electron oxidation intermediate, cation free-radical) and at 450 nm (two-electron oxidation product, diimine), respectively.²⁰ Thus we can facilely monitor the progress of oxidation using the routine UV–vis spectroscopy technique. Our examinations in Figure 1a,b (also see Figure S2) reveal that the TMB molecules

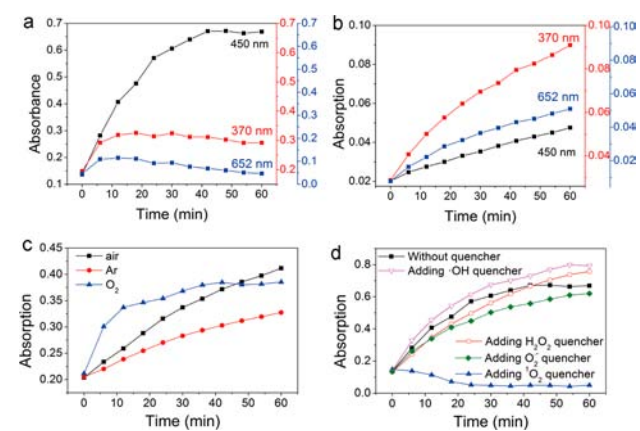


Figure 1. Curves for absorbance of TMB oxidation products at 370, 450, and 652 nm versus reaction time, reflecting the trends for producing intermediate and final products with (a) Pd nanocubes and (b) Pd octahedrons. Trend for producing the final product with Pd nanocubes (c) in different gas environments and (d) in the presence of various scavenger molecules.

can be oxidized when they are mixed with Pd nanocrystals without the need of introducing additional oxidants, such as peroxides. Notably the reactions exhibit much higher rates than that by hydrogen peroxide at 10 °C (see Figure S3). Although both the Pd nanocubes and octahedrons can induce the oxidation of TMB molecules, differentiated strength of oxidation has been observed when TMB solution is mixed with different Pd nanocrystals; addition of nanocubes leads to the formation of final two-electron products, while octahedrons mainly yield one-electron intermediates. As a result, distinct color changes are well resolved in solution, as shown in Figure S2c; the blue color corresponds to the absorption at 652 nm by the octahedrons, and the yellow-green represents those at 450

nm plus 652 nm by the nanocubes. The Ar- and O_2 -purged TMB reactions further confirm that the oxidation of TMB molecules is caused by species evolved from O_2 , as the oxidation rate is highly dependent on the environmental oxygen concentration (see Figure 1c). Taken together, the results reveal that both the two nanostructures can generate active oxygen species from the O_2 dissolved in water but exhibit different activation activities.

Since it is clear that O_2 can be activated to form oxidative species with Pd nanocrystals, it is imperative to clarify what species is actually generated to provide the oxidative function. In principle, O_2 can be activated to form a variety of reactive oxygen species including superoxide (O_2^-), hydrogen peroxide (H_2O_2), hydroxyl radicals ($OH\cdot$) and singlet oxygen (1O_2), each of which may play an important role in chemical reactions and biological systems.²¹ In order to identify the type of species generated in our system, we employ the scavenger mechanism to examine the system. It has been well established that carotene, mannite, catalase, and SOD are specific scavengers that can effectively inhibit the generation of 1O_2 , $OH\cdot$, H_2O_2 , and O_2^- species, respectively.^{21–23} Figure 1d shows the trend for oxidizing the TMB molecules with Pd nanocubes in the presence of various scavengers. Among the various scavengers, only carotene effectively inhibits the TMB oxidation, suggesting that the active species generated on the surface of Pd nanocrystals is singlet oxygen 1O_2 .

In order to further confirm the production of singlet oxygen, we have employed 4-oxo-TMP as a 1O_2 -sensitive trapping agent to examine the system using ESR spectroscopy. 4-oxo-TMP has been commonly used as a sensitive probe for singlet oxygen. The interaction of 4-oxo-TMP with 1O_2 produces stable nitroxide radical 4-oxo-TEMPO that can have characteristic signals in ESR spectroscopy (see Figure S4).²⁴ In the measurements, the ESR signals for both the Pd nanocubes and octahedrons (Figures 2a) clearly display a 1:1:1 triplet

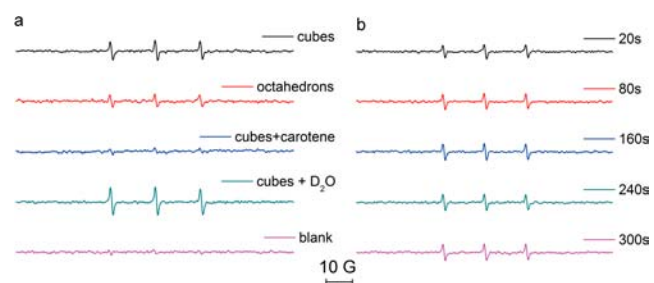


Figure 2. ESR spectra of the samples after mixing 4-oxo-TMP solution with Pd nanocrystals in different conditions: (a) nanocubes in H_2O , octahedrons in H_2O , nanocubes in the presence of carotene, nanocubes in H_2O with 50 μ L D_2O , and a background curve collected from 4-oxo-TMP solution alone, respectively; (b) nanocubes under irradiation of UV light source ($\nu < 400$ nm) for different time (20–300 s).

characteristic with a g -value of 2.0055 and a hyperfine splitting constant ($hfsc$, $aN = 1.604$ mT), which are consistent with those for 4-oxo-TEMPO in literature.²⁴ It verifies that singlet oxygen is formulated via the addition of Pd nanocrystals. Although both the two nanostructures can induce the formation of singlet oxygen, the intensity of 4-oxo-TEMPO signal in the case of nanocubes is significantly higher than that with octahedrons. It further confirms that the $\{100\}$ facets can more easily produce singlet oxygen, as compared with the

{111} facets. The formation of singlet oxygen in our system is also proven by the control experiments in the presence of D₂O or carotene. Note that D₂O is a useful chemical that can prolong the lifetime of singlet oxygen.¹⁶ The results clearly demonstrate that the signal of 4-oxo-TEMPO can be enhanced by D₂O and quenched by carotene in both the cases of Pd nanocubes and octahedrons (see Figures 2a and S5), suggesting that the species appearing in our system is singlet oxygen indeed.

Given that the species has been determined to be ¹O₂, it is fundamentally interesting to elucidate the mechanism behind: What factor induces the change in the electron spin state of O₂? The LSPR sensitization mechanism has been tentatively employed as an explanation for the generation of singlet oxygen with metal nanoparticles in literature;^{1,16} however, it remains largely elusive why the spin-flip process could occur during the LSPR energy harvesting, since this process should be inhibited by the spin selection rule.^{12,13} In order to assess whether the LSPR plays a role in promoting the ¹O₂ production, we have examined the system using the ESR 4-oxo-TMP probing technique under irradiation of different light sources. It is well-known that the LSPR band of 6–21 nm Pd nanocrystals is located in the UV region,¹⁷ so it is supposed that the ¹O₂ production should be facilitated under the UV irradiation if the LSPR “sensitization” mechanism is responsible for the ¹O₂ production. Surprisingly, the signal of 4-oxo-TEMPO is not promoted by the illumination of UV light, indicating that the formation of ¹O₂ does not gain energy from LSPR light harvesting (see Figures 2b). Under the illumination of visible light, the signal of 4-oxo-TEMPO can be enhanced about 100% when the measurement is performed without thermostatic adjustment. However, when the temperature is maintained at 20 °C with a thermostatic device, the enhancement of 4-oxo-TEMPO signal is shown very minimal (see Figure S6). Thus we can conclude that the promotion of ¹O₂ production by visible light is mainly caused by a thermal effect. Overall, the LSPR mechanism should not be responsible for the spin-flip process, as the LSPR band of Pd nanocrystals is located in UV region.

Since the oxygen activation into ¹O₂ is irrelevant to the LSPR, we have to reexamine the nature of Pd nanocrystals from the viewpoint of their direct interactions with O₂. Both the TMB and 4-oxo-TMP measurements above have shown that the O₂ activation is so sensitive to the morphologies of Pd nanocrystals. For this reason, transmission electron microscopy (TEM) has been employed to examine the structures of the Pd nanocrystals that are used in our studies. The TEM images (Figure 3a,b) clearly show that the two samples of Pd nanocrystals have cubic and octahedral shapes with an average edge length of 14 and 6 nm, respectively. Figure 3c,d shows high-resolution TEM (HRTEM) images of the nanocrystals, identifying that the nanocubes and octahedrons are enclosed by {100} and {111} facets, respectively. Thus the shape-dependent activities of activating O₂ on the nanocubes and octahedrons may be actually caused by a facet effect: The {100} facets have a stronger capability of generating active oxygen species than the {111} facets. According to the calculations in Table S1, the percentages of surface atoms for nanocubes and octahedrons are 8.22% and 23.87%, respectively. In our investigations, we adjust the concentrations of nanocrystals to maintain an equivalent number of surface atoms for molecular activation and catalysis.

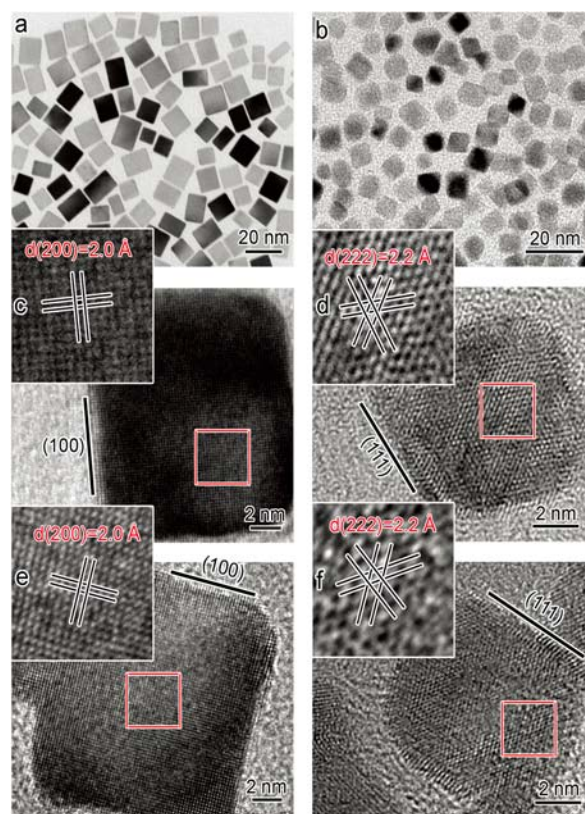


Figure 3. TEM and HRTEM images of the Pd (a,c) nanocubes and (b,d) octahedrons used in the investigations. (e,f) HRTEM images of the Pd nanocrystals after the reactions of glucose oxidation.

Based on the findings above, the major question for mechanism studies arises: Why surface facet of Pd nanocrystals has a huge impact on the oxygen activation? It is known that the interaction of small molecules with crystallographic facets is mainly determined by molecular adsorption. For this reason, we employ theoretical simulations to elucidate the impact of adsorption on the oxygen activation. In the simulations, we examine the adsorption state of molecular oxygen on different facets of Pd and analyze whether the adsorption process affects the spin state of electrons in oxygen molecules. All calculations were performed using the PAW method, with the PBE as recently implemented in VASP code. In the simulation, we have considered several configurations for the chemisorbed O₂ molecular with different interatomic distances optimized as shown in Figures S7 and S8. As a result, we can acquire the values for the adsorption energy of O₂ in each configuration (see Tables S2 and S3). According to the adsorption energy, the most favorable configuration on Pd(100) is shown in Figure 4a–c, where the O₂ is chemisorbed on the hollow site confined by four neighbor Pd atoms. The magnetic moment of chemisorbed O₂ molecules on Pd(100) is 0.017 μ_B , which is 1.983 μ_B lower than the free O₂ molecules.²³ In contrast, the most favorable configuration on Pd(111) is the O₂ chemisorbed on the bridge site confined by two neighbor Pd atoms (see Figure 4e–g). The magnetic moment of chemisorbed O₂ molecules on Pd(111) is 0.549 μ_B , which is 1.451 μ_B lower than the free O₂ molecules and 32 times higher than that of the O₂ molecules on Pd(100). Hence, the molecular O₂ is more activated on Pd(100) crystal surface than on Pd(111), in terms of the decrease in the magnetic moment of O₂. The significant reduction of magnetic moment to nearly

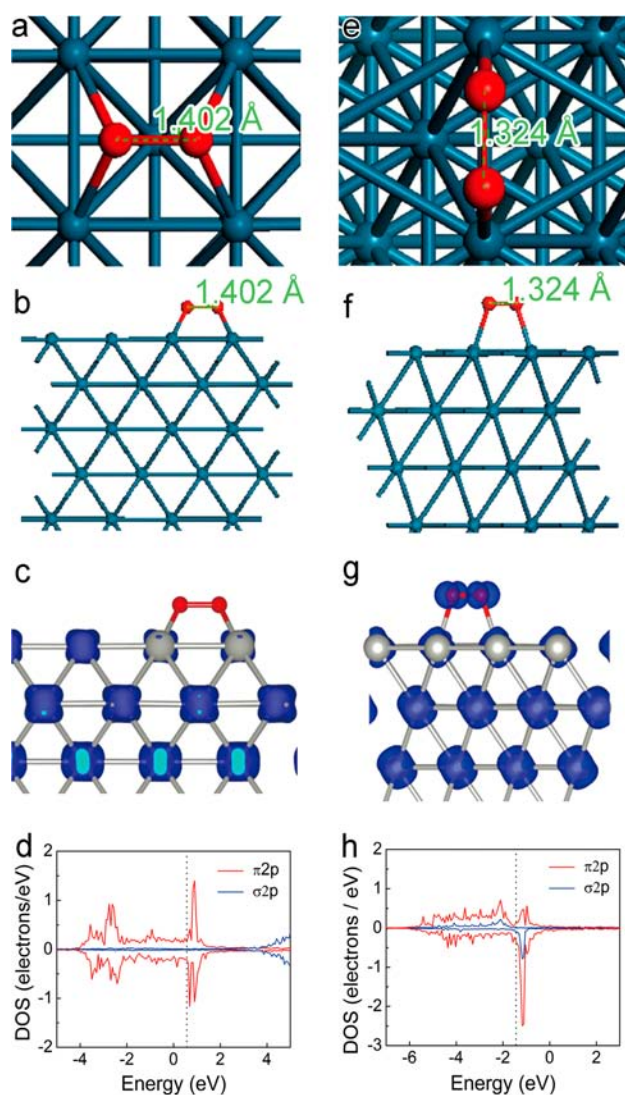


Figure 4. The most favorable adsorption configurations of O_2 on Pd(100) facet: (a) top view, (b) side view, and (c) spin charge density; and Pd(111) facet: (e) top view, (f) side view, and (g) spin charge density. The projected density of states (PDOS) diagrams of (d) O_2 adsorbed on Pd(100) in the configuration and (h) O_2 adsorbed on Pd(111) in the configuration. The dashed lines denote the Fermi level. The isovalue of spin charge density is 0.01.

zero, in the case of O_2 on Pd(100), indicates the perfect spin-flip process upon the chemisorption onto Pd(100). More careful examination on the electron density of O_2 reveals significant electron transfer (about 0.7 electron charge) from Pd(100) surface to molecular oxygen. In comparison, the charge transfer from Pd(111) to O_2 is ~ 0.4 electron charge, which is less than that from Pd(100) surface. The significant electron transfer occurring on the Pd(100) surface should be the primary mechanism responsible for oxygen activation during the chemisorption. It is well-known that the magnetism of O_2 molecule comes from the two nonpaired electrons in the frontier π^* orbital of O_2 molecule. The transferred electrons from Pd surface to O_2 molecule will occupy its antibonding π^* orbital, leading to the spin reduction on O_2 molecule. This picture is also confirmed by the calculated spin charge distribution profiles and density of states (DOS) projected on O's atomic orbital. As shown in Figure 4c,g, there is distinct spin charge distribution on O_2 molecule for Pd(111) surface,

whereas no distribution on O_2 molecule is observed for Pd(100) surface. The magnetic moment of O atom is mainly contributed by the O's 2p orbital (see Figure 4h).

The charge transfer from Pd to frontier antibonding orbital of O_2 molecule also leads to the elongation of O–O bond. From the most favorable configurations, one can see that the O_2 on Pd(100) crystal surface possesses a slightly larger bond length than that on Pd(111) (1.402 versus 1.324 Å), also suggesting the better activation of O_2 on Pd(100). To examine the adsorption state of O_2 on Pd surface experimentally, we have collected near-edge X-ray absorption fine structure (NEXAFS) spectroscopy spectra of O_2 adsorbed on the Pd nanocubes and octahedrons, respectively (see Figure S10). The resonance at 530.9 eV can be assigned to $1\sigma_u \rightarrow 1\pi_g^*$ transition for the chemisorption of O_2 on Pd surface.²⁵ The shoulder peak next to the chemisorption of O_2 on Pd(100) shifts to lower energy in contrast to O_2 on Pd(111), indicating that the bond length of O_2 on the nanocubes [i.e., Pd(100)] is slightly longer than that on the octahedrons [i.e., Pd(111)] according to the well-established Natoli's rule.²⁶ Such a conclusion is consistent with the simulation findings, supporting that our simulation results are reasonable. The DOS of O_2 on Pd(100) and Pd(111) obtained from the calculation is shown in Figure 4d,h. It reveals that the electronic densities of O_2 are significantly altered upon the chemisorption of O_2 onto Pd surface accompanying the orbital hybrid of O and Pd atoms, in comparison with the DOS of free O_2 (Figure S11). The varied DOS on Pd(100) and Pd(111) contributes to the different magnetic moment of O_2 on their surface, thus definitely differentiating their capabilities in molecular activation.

It is worth pointing out that the adsorption of oxygen to palladium surface is a spontaneous process without energy barrier, as one can see from the pathway of energy evolution during the adsorption (Figure S9). The total energy evolution profile versus the vertical distance (between O_2 molecule and Pd surface) for O_2 adsorption on Pd(100) surface is obtained by fixing the vertical distance between the O_2 molecule and Pd(100) surface when performing each structural optimization and manually reducing this distance from 3.78 to 2.14 Å step by step. Thus the process of oxygen adsorption should be mainly governed by thermodynamics. On the other hand, although the most favorable configuration in Figure 4a is determined by adsorption energies in the simulations, it still represents the most active species of oxygen among various configurations according to their magnetic moments (see Tables S2 and S3). In practice, it would be the most possible pathway that O_2 is activated to react with chemicals in various reactions. Overall, from the viewpoint of both the adsorption step and oxidation reaction, kinetics should not be a major focus to alter the reaction pathway in our case.

Enabled by their different capabilities of producing singlet oxygen, we have been able to investigate the performance of Pd nanocubes and octahedrons in catalyzing glucose oxidation (Figure S12).²⁷ As shown in Table 1, both the two Pd structures can catalyze the oxidation of glucose, regardless of their variable efficiencies. In order to clarify the role of singlet O_2 in the reaction, we have performed the glucose oxidation using Pd nanocubes in the presence of carotene (i.e., the scavenger for singlet O_2), which shows only 1% yield of gluconic acid. It exclusively demonstrates that the glucose oxidation proceeds via the function of generating singlet O_2 , so the efficiency of Pd nanocrystals in catalyzing the reaction should be determined by the step of O_2 adsorption and

Table 1. Oxidation of Glucose by Pd Nanocrystals with Molecular Oxygen^a

catalyst	mol _{surf} %	mol _{total} %	mol _{e,c} %	yield % ^b	TON _{surf}	TON _{total}
14 nm nanocubes	1.6	2.0	0.05	85	516	42
14 nm nanocubes ^c	1.6	2.0	0.05	1	8	1
6 nm octahedrons	1.6	0.7	0.22	35	214	51
7 nm nanocubes	1.6	1.0	0.08	86	553	85
7 nm nanocubes	3.1	2.0	0.17	99	323	50
20 nm nanocubes	1.6	2.7	0.03	88	545	32
20 nm nanocubes	1.2	2.0	0.02	48	413	25
21 nm octahedrons	1.6	2.2	0.06	33	209	15
21 nm octahedrons	0.5	0.7	0.02	13	262	19
none ^d				0	–	–

^aReaction conditions: glucose in H₂O as solvent (15 mM) and maintain pH = 9 by adding sodium hydroxide during reaction, 50 °C, O₂ (10 mL/min), 120 min. ^bDetermined by HPLC analysis via an internal standard technique. ^cAddition of 4 mg carotene as ¹O₂ scavenger. ^dReaction time: 960 min.

activation which can be modulated by their surface facets. As expected, Pd nanocubes exhibit much better performance than octahedrons at the same concentration in terms of surface atoms, observed from both the yield and turnover numbers (TON). For instance, at the surface atom percentage of 1.6%, the yield and TON using Pd nanocubes can reach 85% and 545, respectively, but those for octahedrons are only 35% and 232, respectively. Even when the usage dose of octahedrons is increased to 2.3%, the yield for gluconic acid can only reach 70% (see Tables S4). Certainly, for each sample, the TON is highly dependent on the usage dose of Pd catalysts. When the dose of Pd nanocubes is as low as 0.04%, their TON in catalyzing glucose oxidation can reach 2016 (see Tables S4).

In order to validate the assumption that the catalytic activities are determined by the number of surface atoms, three different sizes of Pd nanocubes (7, 14, and 20 nm in edge length) and two sizes of octahedrons (6 and 21 nm in edge length, Figure S13) are used as catalysts in the oxidation of glucose, respectively. When the mol ratios of surface atoms are set as 1.6%, the yields for gluconic acid are identical with the nanocubes at different sizes as catalysts. The same observation has been also obtained in the case of octahedrons. It indicates that the number of surface atoms is the most important parameter to determine the catalytic activities of catalysts in our case. Note that the number of atoms at the corners and edges is dramatically reduced with increase of particle size, as one can see from Table 1. However, the catalytic efficiency can be retained while altering the particle size, as long as the concentration in terms of surface atoms is maintained constant. This observation clearly excludes the possibility that the atoms at the sites of corners and edges play the key role in activating molecular oxygen. On the other hand, when normalized by the number of total atoms, the yields for glucose oxidation increase as the nanocubes are down-sized. At the surface atom percentage of 3.2%, the use of 7 nm nanocubes can achieve a yield of 99%. It is mainly ascribed to the increase in their

surface-to-volume ratios. This series of investigations clearly verifies the validity of our quantification criteria in assessing the catalytic activities of samples.

Similar to the finding in the 4-oxo-TMP probing system, the yield for glucose oxidation cannot be promoted by the UV light (see Table S5). It again verifies that the activation of molecular oxygen is not ascribed to the “LSPR sensitization” mechanism. The HRTEM images in Figure 2e,f reveal that the interactions of Pd nanocrystals with O₂ in the glucose oxidation do not induce noticeable morphological changes in the catalysts (also see TEM images in Figure S14). It suggests that the Pd nanocrystals can be recycled for sustainable usage in related catalytic reactions.

Another application of ¹O₂ generation is cancer treatment. For instance, ¹O₂ has been proven as a class of important species to damage the cancer cells in the photodynamic therapy (PDT) treatment of cancer.^{28–31} In the past research, the facet effect of metal nanocrystals on the cancer treatment has been somehow ignored. Herein we have investigated the capabilities of different Pd facets in reducing the viability of cancer cells. As shown in Figure 5, {100} facet-covered Pd nanocubes could

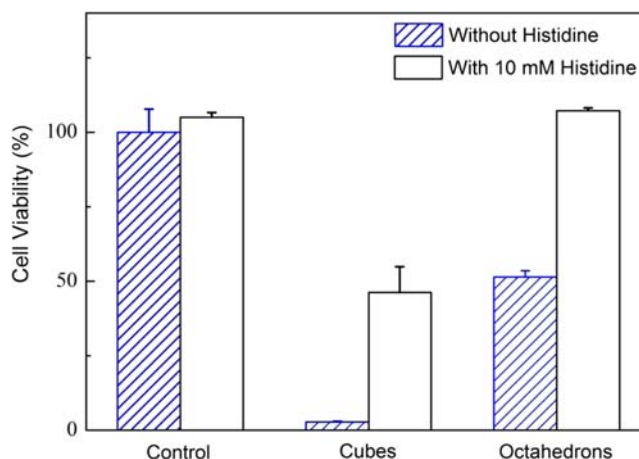


Figure 5. Viability of human HeLa cancer cells that were incubated with palladium nanocrystals at the same concentration in terms of surface atoms for 24 h. Cell viabilities were measured by the standard 3-(4,5-dimethylthiazol-2-yl)-2,5-diphenyltetrazolium bromide (MTT) assay. In order to verify the role of ¹O₂ in cancer treatment, the scavenger for ¹O₂ species histidine was added in a control experiment. Error bars were based on triplet measurements.

completely kill the HeLa cancer cells (10 000 cells/well) after incubation for 24 h. In contrast, the viable cell count was reduced by only 50% with the treatment by Pd octahedrons enclosed by {111} facets at the same concentration of surface atoms. In order to verify whether this difference is caused by ¹O₂ generation, we have performed a control experiment using histidine. Histidine has been proven as an efficient scavenger for ¹O₂ species,³² and the control experiment has clarified that histidine alone does not reduce the cell viability. In the presence of histidine, both the Pd nanocubes and octahedrons could not kill the cancer cells, confirming that the cells were damaged by ¹O₂ species produced from Pd nanocrystals indeed. Noble metal nanocrystals have been widely explored for their function in cancer treatment; however, no sufficient attention is being paid to the facet effect when designing the cancer treatment agents with the nanocrystals.^{33–36} This investigation clearly shows that facet control should represent a route to

precisely design the capability of metal nanocrystals in cancer treatment.

CONCLUSION

In conclusion, we have demonstrated that the surface facet of metal nanocrystals is a key parameter for tuning their activities of generating singlet oxygen. By excluding the role of LSPR in promoting the spin–flip process, we investigate the effect of surface facets on the oxygen activation both experimentally and theoretically. The mechanism studies suggest that surface facets may alter the chemisorption state of oxygen on metal surface and, in turn, causes the changes in the magnetic moment (i.e., spin state) of oxygen through electron transfer from Pd surface to O₂. When appropriate surface facets are selected, a spontaneous spin–flip process may occur during the chemisorption process. Since oxygen activation is a critical step in many organic reactions considering the spin selection rule, the facet-dependent activities of metal nanocrystals presented here provide guidance for designing high-performance catalysts for organic reactions. As a demonstration, we have verified that {100} facet-enclosed Pd nanocubes exhibit superior catalytic performance to {111} octahedrons in glucose oxidation. Another perspective of this work is the controllability in tailoring the cancer treatment materials for high ¹O₂ production efficiency, based on the facet control of metal nanocrystals. As a proof-of-concept experiment, we have demonstrated that Pd(100) can provide better capability of cancer treatment than Pd(111). Although Pd is not an ideal material for biocompatible applications, it is anticipated that this finding will pave a new way for designing cancer therapy agents by tailoring the surface facets of other metal nanostructures.

ASSOCIATED CONTENT

Supporting Information

Detailed experimental section, characterization, and calculation methods, and additional material characterizations. This material is available free of charge via the Internet at <http://pubs.acs.org>.

AUTHOR INFORMATION

Corresponding Author

yjxiong@ustc.edu.cn

Notes

The authors declare no competing financial interest.

ACKNOWLEDGMENTS

This work was financially supported by the National Natural Science Foundation of China (NSFC) (no. 21101145), the Recruitment Program of Global Experts and the CAS Hundred Talent Program. We thank Prof. Jiafu Chen for his assistance in the ESR measurements and discussions of the ESR data. X.W. is supported by the National Basic Research Programs of China (nos. 2011CB921400, 2012CB922001), the NSFC (nos. 21121003, 11004180, 51172223), the CAS Hundred Talent Program, the Shanghai Supercomputer Center, and the Hefei Supercomputer Center.

REFERENCES

- (1) Christopher, P.; Xin, H.; Linic, S. *Nat. Chem.* **2011**, *3*, 467–472.
- (2) Acevedo, O. L.; Kacprzak, K. A.; Akola, J.; Häkkinen, H. *Nat. Chem.* **2010**, *2*, 329–334.

- (3) Xie, X.; Li, Y.; Liu, Z.; Haruta, M.; Shen, W. *Nature* **2009**, *458*, 746–749.
- (4) Hughes, M. D.; Xu, Y.; Jenkins, P.; McMorn, P.; Landon, P.; Enache, D. I.; Carley, A. F.; Attard, G. A.; Hutchings, G. J.; King, F.; Stitt, E. H.; Johnston, P.; Griffin, K.; Kiely, C. J. *Nature* **2005**, *437*, 1132–1135.
- (5) Kesavan, L.; Tiruvalam, R.; Rahim, M. H. A.; Saiman, M. I. B.; Enache, D. I.; Jenkins, R. L.; Dimitratos, N.; Lopez-Sanchez, J. A.; Taylor, S. H.; Knight, D. W.; Kiely, C. J.; Hutchings, G. J. *Science* **2011**, *331*, 195–199.
- (6) Enache, D. I.; Edwards, J. K.; Landon, P.; Solsona-Espriu, B.; Carley, A. F.; Herzing, A. A.; Watanabe, M.; Kiely, C. J.; Knight, D. W.; Hutchings, G. J. *Science* **2006**, *311*, 362–365.
- (7) Wittstock, A.; Zielasek, V.; Biener, J.; Friend, C. M.; Bäumer, M. *Science* **2010**, *327*, 319–322.
- (8) Mori, K.; Hara, T.; Mizugaki, T.; Ebitani, K.; Kaneda, K. *J. Am. Chem. Soc.* **2004**, *126*, 10657–10666.
- (9) Holland, J. T.; Lau, C.; Brozik, S.; Atanassov, P.; Banta, S. *J. Am. Chem. Soc.* **2011**, *133*, 19262–19265.
- (10) Ishida, T.; Kinoshita, N.; Okatsu, H.; Akita, T.; Takei, T.; Haruta, M. *Angew. Chem., Int. Ed.* **2008**, *47*, 9265–9268.
- (11) Hirota, M.; Furihata, K.; Saito, T.; Kawada, T.; Isogai, A. *Angew. Chem., Int. Ed.* **2010**, *49*, 7670–7672.
- (12) Wahlen, J.; De Vos, D. E.; Jacob, P. A.; Alsters, P. L. *Adv. Synth. Catal.* **2004**, *346*, 152–164.
- (13) Kovalev, D.; Fujii, M. *Adv. Mater.* **2005**, *17*, 2531–2544.
- (14) Schweitzer, C.; Schmidt, R. *Chem. Rev.* **2003**, *103*, 1685–1758.
- (15) Nirmal, M.; Norris, D. J.; Kuno, M.; Bawendi, M. G. *Phys. Rev. Lett.* **1995**, *75*, 3728–3731.
- (16) Vankayala, R.; Sagadevan, A.; Vijayaraghavan, P.; Kuo, C.-L.; Hwang, K. C. *Angew. Chem., Int. Ed.* **2011**, *50*, 10640–10644.
- (17) Xiong, Y.; Chen, J.; Wiley, B.; Xia, Y.; Yin, Y.; Li, Z. *Nano Lett.* **2005**, *5*, 1237–1242.
- (18) Pal, R.; Wang, L. M.; Pei, Y.; Wang, L. S.; Zeng, X. C. *J. Am. Chem. Soc.* **2012**, *134*, 9438–9445.
- (19) Li, B.; Long, R.; Zhong, X.; Bai, Y.; Zhu, Z.; Zhang, X.; Zhi, M.; He, J.; Wang, C.; Li, Z.-Y.; Xiong, Y. *Small* **2012**, *8*, 1710–1716.
- (20) Joseph, P. D.; Eling, T.; Mason, R. P. *J. Biol. Chem.* **1982**, *257*, 3669–3675.
- (21) Badwey, J. A.; Karnovsky, M. L. *Annu. Rev. Biochem.* **1980**, *49*, 695–726.
- (22) Barnese, K.; Gralla, E. B.; Cabelli, D. E.; Valentine, J. S. *J. Am. Chem. Soc.* **2008**, *130*, 4604–4606.
- (23) Rao, P. S.; Luber, J. M.; Milinowicz, J.; Lalezari, P.; Mueller, H. S. *Biochem. Biophys. Res. Commun.* **1988**, *150*, 39–44.
- (24) Konaka, R.; Kasahara, E.; Dunlap, W. C.; Yamamoto, Y.; Chien, K. C.; Inoue, M. *Free Radical Biol. Med.* **1999**, *27*, 294–300.
- (25) Wurth, W.; Stöhr, J.; Feulner, P.; Pan, X.; Bauchspiess, K. R.; Baba, Y.; Hudel, E.; Rocker, G.; Menzel, D. *Phys. Rev. Lett.* **1990**, *65*, 2426–2429.
- (26) Natoli, C. R. Near Edge Absorption Structure in the Framework of the Multiple Scattering Model. Potential Resonance or Barrier Effects? In *EXAFS and Near Edge Structure*, Bianconi, A., Incoccia, L., Stipich, S., Eds.; Springer: Berlin Heidelberg, Germany, 1983; Vol. 27, pp 43–56.
- (27) Besson, M.; Lahmer, F.; Gallezot, P.; Fuertes, P.; Fleche, G. *J. Catal.* **1995**, *152*, 116–121.
- (28) Dolmans, D. E. J. G. J.; Fukumura, D.; Jain, R. K. *Nat. Rev. Cancer* **2003**, *3*, 380–387.
- (29) Lovell, J. F.; Liu, T. W. B.; Chen, J.; Zheng, G. *Chem. Rev.* **2010**, *110*, 2839–2857.
- (30) Ogilby, P. R. *Chem. Soc. Rev.* **2010**, *39*, 3181–3209.
- (31) Idris, N. M.; Gnanasamandhan, M. K.; Zhang, J.; Ho, P. C.; Mahendran, R.; Zhang, Y. *Nat. Med.* **2012**, *18*, 1580–1585.
- (32) Das, K.; Das, C. *Biochem. Biophys. Res. Commun.* **2000**, *277*, 443–447.
- (33) Murphy, C. J.; Gole, A. M.; Stone, J. W.; Sisco, P. N.; Alkhalany, A. M.; Goldsmith, E. C.; Baxter, S. C. *Acc. Chem. Res.* **2008**, *41*, 1721–1730.

- (34) Huang, X.; Tang, S.; Mu, X.; Dai, Y.; Chen, G.; Zhou, Z.; Ruan, F.; Yang, Z.; Zheng, N. *Nat. Nanotechnol.* **2010**, *6*, 28–32.
- (35) Xia, Y.; Li, W.; Cobiey, C. M.; Chen, J.; Xia, X.; Zhang, Q.; Yang, M.; Cho, E.; Brown, P. K. *Acc. Chem. Res.* **2011**, *44*, 914–924.
- (36) Barhhan, R.; Lal, S.; Joshi, A.; Halas, N. J. *Acc. Chem. Res.* **2011**, *44*, 936–946.